Marine Pollution Bulletin 209 (2024) 117085

Contents lists available at ScienceDirect

Marine Pollution Bulletin

journal homepage: www.elsevier.com/locate/marpolbul

Assessment of nutrient cycling in an intensive mariculture system

Yanmin Wang, Xianghui Guo, Guizhi Wang, Lifang Wang, Tao Huang, Yan Li, Zhe Wang, Minhan Dai *

State Key Laboratory of Marine Environmental Science, College of Ocean and Earth Sciences, Xiamen University, Xiamen 361102, China

ARTICLE INFO

Keywords:
Nutrient release
Trash fish feed
Formulated feed
Integrated multi-trophic aquaculture
Sansha Bay

ABSTRACT

Rapid mariculture expansion has raised concerns about coastal eutrophication. This study assesses nutrient cycling in Sansha Bay, China, a eutrophic semi-enclosed bay with intensive mariculture. A two-endmember mixing model showed significant additions of dissolved inorganic nitrogen (DIN; 6.9 ± 4.1 μmol L^{-1}) and phosphorus (DIP; 0.45 ± 0.29 μmol L^{-1}) in May 2020, mainly from mariculture. Estimated N and P inputs from fish farming were 7789 ± 361 tons and 1497 ± 91 tons in spring, respectively, with N mainly in dissolved form and P in particulate form. And, trash fish feed caused higher nutrient release than formulated feed. Of the feed input, 52.8 ± 4.7 % of DIN and 33.0 ± 3.7 % of DIP were released into environment, exceeding riverine input and offshore exchanges. Co-culturing kelp and oysters removed 1079 ± 11 tons of N and 156 ± 8 tons of P. Therefore, adjusting feed types and planning co-cultivation strategies could alleviate eutrophication resulting from mariculture expansion.

1. Introduction

The global demand for aquatic products over the past decades has fueled the rapid development of coastal aquaculture, making it the fastest growing sector of food production worldwide (Subasinghe et al., 2009; Chen and Qiu, 2014). Global aquaculture production has increased by approximately 600 %, from 1.73 × 10^7 tons in 1990 to 1.20 × 10^8 tons in 2019 (FAO, 2021). Mariculture accounts for ~48 % of total aquaculture production with a growth rate of 2.36 × 10^6 tons yr^{-1}, which outcompetes that of freshwater culture (1.92 × 10^6 tons yr^{-1}) over the past decade (FAO, 2021). Notably, China emerged as the largest global aquaculture producer since 1989, contributing to ~57 % of total world production in 2019, i.e., a tenfold increase over the past two decades (FAO, 2021). This growth trend is expected to continue globally, most notably in developing countries (Diana et al., 2013).

Mariculture development has indeed provided great economic and social benefits; however, cage farming has been reported to contribute additional pressures to the already impacted coastal marine environment, notably manifested by eutrophication, harmful algal blooms (HABs), and hypoxia (e.g., Anderson et al., 2002; Cao et al., 2015; Breitburg et al., 2018; Dai et al., 2023). Indeed, many studies have reported instances of eutrophication in waters used for mariculture (e.g., Schneider et al., 2005; Skriptsova and Miroshnikova, 2011; Wang et al., 2012; Bouwman et al., 2013). One commonly cited factor contributing to this problem is the high feed conversion rate (R_{conv}, the amount of feed required to produce 1 kg of wet weight fish product), i.e., the low utilization efficiency of fish feed (Nederlof et al., 2021). For example, the Norwegian salmon farming industry has taken important steps to reduce the R_{conv} value. However, approximately 58–62 % of N and 79–81 % of P from the total feed input in Norwegian farming industry were still released into the environment when the R_{conv} ranged between 1.06 and 1.17 (Wang and Olsen, 2023). These unutilized nutrients are either released into the water column in dissolved form or deposited on the seafloor in particulate form, eventually altering the aquatic and sedimentary environment, especially in closed and semi-enclosed bays where water exchange is limited. Moreover, mariculture can lead to diverse environmental impacts. For example, He et al. (2022) reported that suspended aquaculture weakens the onshore current near the aquaculture boundary and upwelling within the offshore aquaculture area, resulting in a reduction of ~60 % in the nutrient supply. Therefore, the effects of mariculture on coastal nutrient dynamics remain inconclusive and quantitatively uncertain. It is necessary to evaluate the amount of released nutrients and the flow and fate of nutrients in different forms within fish farming system.

A new development to increase sustainability in the mariculture sector is the adoption of an integrated multi-trophic aquaculture (IMTA) approach (e.g., Chopin et al., 2012; Jiang et al., 2012; Wu et al., 2015; Granada et al., 2016; Wei et al., 2017; Campanati et al., 2021).

* Corresponding author.
E-mail address: mdai@xmu.edu.cn (M. Dai).

https://doi.org/10.1016/j.marpolbul.2024.117085
Received 13 August 2024; Received in revised form 20 September 2024; Accepted 30 September 2024
Available online 12 October 2024

Macroalgal cultivation is often included in the IMTA system as an ecologically friendly option to alleviate environmental impacts. It plays a crucial role in nutrient recycling and transformation, primarily due to its pronounced capacity for nutrient absorption and storage in tissues (e.g., Yang et al., 2006; Marinho-Soriano et al., 2009). Bivalves provide another effective trophic pathway for the removal of suspended particles from the water in the IMTA system, leading to the conversion of nutrient wastes into biomass (Martinez-Porchas and Martinez-Cordova, 2012; Carboni et al., 2016). Although these studies assessed the purification effects of macroalgae and bivalves on the mariculture environment, they ignored how mariculture activities affect the nutrient balance of the entire marine ecosystem. In practice, it is necessary not only to evaluate the impacts of the IMTA system on nutrient cycling based on feed types, the cultivation species and the feeding strategy, but also to consider the nutrient budget of the entire study area by integrating river input and exchange with offshore coastal waters.

We focus here on Sansha Bay, possibly the highest-density IMTA system worldwide. This system features the world's largest cage culture of large yellow croaker (*L. crocea*) (Song et al., 2023). We examine the variation in nutrient characteristics during the spring season, a critical period when environmental parameters such as nutrients and temperature variations can easily lead to HABs, especially in mariculture areas (e.g., Huo et al., 2018; Xie et al., 2020). We show the nutrient sources, distributions, and releases in this complex and highly impacted system to provide a scientific basis for assessing the role of mariculture as a driver of changes in the coastal environment and to support decision-making towards a more sustainable model. By establishing a mass balance of N and P, we assess the release of nutrients from the fish farming system using different feeds. We also analyze the external nutrient input/removal in this ecosystem, affected by intensive mariculture (fish, kelp and oyster farming), riverine input, and exchange with offshore coastal waters.

2. Materials and methods

2.1. Study area

Sansha Bay, located on the northeast coast of Fujian Province, China, is a semi-enclosed bay comprised of several secondary bays, such as Baima Harbor, Yantian Harbor, Dongwuyang, Guanjingyang, and Sandu'ao (Fig. 1) (Lin et al., 2017). The surface area of the bay is ~675 km^2 (Lin et al., 2016; Han et al., 2021), with a tortuous 553 km coastline (Yan and Cao, 1997). It has only one outlet, ca. 2.9 km wide, to the southern East China Sea (ECS) (Wang et al., 2018), and the water depth within the bay ranges from a few meters to 90 m. Sansha Bay is surrounded by mountains with outcroppings of medium acidic volcanic rocks (Yan and Cao, 1997). It receives several mountain rivers, among which the Jiaoxi Stream provides the largest runoff. In spring 2020 (May), the freshwater discharge of the Jiaoxi Stream was 71.3 $m^3\ s^{-1}$ (data from Nengwang Chen, Xiamen University). This region experiences prevailing seasonal monsoons, influenced by the winter northeast wind and the summer southwest wind. As a result, the bay waters are a dynamic mixture of the China Coastal Current (CCC), the Taiwan Warm Current (TWC), and the South China Sea Warm Current (SCSWC), with seasonal variations in their proportions (e.g., Yang et al., 2008; Qi et al., 2016; Huang et al., 2019; Zhang et al., 2022). Due to its unique geographical features, Sansha Bay has historically served as a naturally sheltered bay (Lin et al., 2017), that fostered the vigorous development of the mariculture industry (Wu et al., 2015; Wei et al., 2017; Xie et al., 2020). However, this development has also influenced the rate and time of water exchange in Sansha Bay. The water exchange is primarily driven by tides, leading to current directions and velocities that are consistent with the tidal patterns (Wu et al., 2015; Lin et al., 2019). The bay is characterized by strong semidiurnal tides, with an average tidal range exceeding 5 m (Lin, 2014) and an average flow rate of 0.5–0.6 m s^{-1} (Wu et al., 2015). Cage culture weakens the overall flow within the bay, but appears to strengthen the water flow among individual cage (Lin et al., 2019). Moreover, studies indicated that the seawater half-exchange time (the time required for half of the bay's seawater to be replaced by offshore coastal waters due to tidal and residual currents) in the main channel is <10 days, while it exceeds 30 days at the head of the bay (Wu et al., 2015; Lin et al., 2017; Lin et al., 2019). However, these hydrodynamic conditions, which are influenced by factors such as river discharge and tides, exhibit seasonal variability, particularly regarding nutrient transport (Lin et al., 2017; Lin et al., 2019). Consequently, this study focuses on assessing the nutrient budget during the spring sampling period, based on the assumption of steady-state conditions (Gordon et al., 1996).

2.2. Maricultural practices and historical changes

Mariculture activities utilize ~69 %[1] of Sansha Bay's surface area. The main cultured species include the *L. crocea*, oyster (*C. gigas*), kelp (*L. japonica*), gracilaria (*G. lemaneiformis*), and others. *L. crocea* is cultured in cages throughout the year, with fish larvae of 2.5–3.0 cm in length introduced into the cages twice a year (April to May and October to December) at a density of about 10,000 per cage (Ji et al., 2021; Liu et al., 2022). As the fish grow, they are regularly sorted into different cages, with densities approaching 600 fish m^{-2} for fish weighing 100–200 g and 160 fish m^{-2} for those weighing 500 g (Liu et al., 2022). Generally, *L. crocea* can reach commercial size within 8–13 months and can be harvested each season depending on market demand. Here, we assume that the production is equal across all four seasons, with the spring production being 4.46×10^4 tons (http://tjj.ningde.gov.cn/xxgk/tjxx/tjnj/). Trash fish feed constitutes the primary bait for breeding *L. crocea*, accounting for ca. 80 % of the feed source (Song et al., 2023). Moreover, the macroalgae are cultivated using suspended lifting ropes in the water, alternating cultivation between kelp and gracilaria from December to May and June to October each year without supplemental feeding (Ji et al., 2021). Kelp is typically harvested in May, with a production of 1.888×10^5 tons during spring (http://tjj.ningde.gov.cn/xxgk/tjxx/tjnj/). Similarly, oysters are cultured year-round in water using raft aquaculture method. Generally, semi-finished seedlings weighing 50–100 g are introduced in October and harvested before the typhoon season (usually in May) the following year, with a production of 1.368×10^5 tons in spring (http://tjj.ningde.gov.cn/xxgk/tjxx/tjnj/).

Based on Landsat and Sentinel-2 remote sensing data from 1999 to 2020, the support vector machine method (detailed in text S1) was employed to classify cage and macroalgal culture distributions. The results showed mariculture gradually expanded from nearshore to offshore waters. Cage culture began sporadically around several islands in deep waters as early as 1999 and then expanded linearly and widely in the nearshore and surrounding areas, while macroalgal culture was scattered throughout the region in 2020 (Fig. 2a). Fig. 2b illustrated the production changes of *L. crocea*, kelp and oyster in this region. The total production of *L crocea* steadily increased from 56 tons in 1990 to 1.785×10^5 tons in 2020. Kelp production showed a similar trend, remaining relatively stable between 1994 and 2006 before gradually increasing. Due to changes in the statistical methodology for oysters, which has included the shell weight since 1997, there was a sudden numerical increase in oyster production. Subsequently, the production showed a declining trend, eventually transitioning into a phase of fluctuating stability starting in 2013 (Fig. 2b). A synthesis of literature data (Table S1) revealed that the concentrations of dissolved inorganic

[1] The percentage is calculated from the mariculture and bay areas in Sansha Bay. The mariculture area was derived from the Ningde Statistical Yearbook (http://tjj.ningde.gov.cn/xxgk/tjxx/tjnj/202111/t20211104_1544289.htm), while the bay area, including both intertidal and water areas, was obtained from Han et al. (2021).

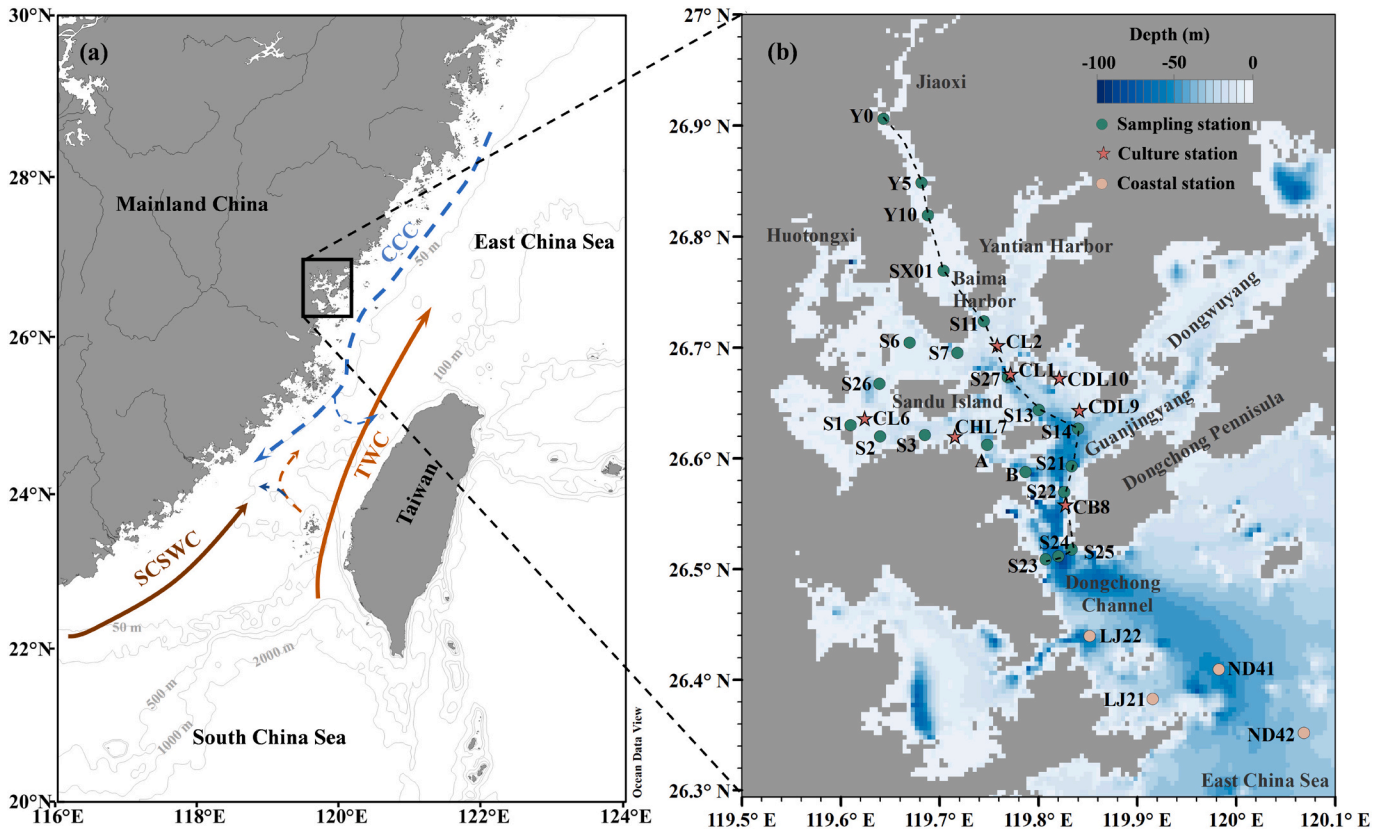

Fig. 1. (a) Map of the study area and schematic of local currents. Blue, brown, and dark brown lines represent the China Coastal Current (CCC), the Taiwan Warm Current (TWC), and the South China Sea Warm Current (SCSWC), respectively. (b) Dark green and pink circles indicate the sampling stations in Sansha Bay and offshore coastal waters during May 2020, with mariculture zones shown as red stars. The black dashed line represents the main channel from Jiaoxi Stream to offshore coastal waters. Bathymetric data are derived from the latest General Bathymetric Chart of the Oceans (GEBCO) grid data. (For interpretation of the references to color in this figure legend, the reader is referred to the web version of this article.)

nitrogen (DIN) and dissolved inorganic phosphorus (DIP) have increased by more than two and three times, respectively, since the 1980s (Fig. 2c). These changes may be attributed to the release of nutrient waste resulting from the mariculture expansion and production growth.

2.3. Sampling and analysis methods

In Sansha Bay, we conducted comprehensive field surveys, sampling, and experiments to analyze nutrients and related parameters. Additionally, we collected biological samples from mariculture zones to measure N and P contents and other relevant parameters.

2.3.1. Sampling and analysis of nutrients and related parameters

The research cruise was conducted onboard the R/V *Funing 11* during May 18–28, 2020. Water temperature and chlorophyll *a* (Chl-*a*) concentrations were measured continuously using a multi-parameter instrument (YSI Model 5065, YSI Co., USA). Discrete water samples for salinity (S) determination were collected using Niskin bottles and analyzed in the laboratory with a portable salinometer (Model Multi 340i, WTW Co., Germany). Simultaneously, water samples for the analysis of nitrate (NO_3^-), nitrite (NO_2^-), ammonium (NH_4^+), phosphate (DIP), silicate ($Si(OH)_4$), and calcium (Ca^{2+}) concentrations were taken and filtered through a 0.45 μm pore size cellulose acetate membrane filter into 125 mL high density polyethylene bottles (Dai et al., 2006; Dai et al., 2008). Nutrient samples, except those for $Si(OH)_4$, were frozen onboard and then measured at a land-based laboratory in Xiamen University. Samples for $Si(OH)_4$ analysis were preserved with 100 μL of chloroform and refrigerated at 4 °C until analysis. Note that the following discussion related to DIN refers to the sum of NO_3^-, NO_2^-, and NH_4^+. Samples for total alkalinity (TA) analysis were stored in 250 mL PYREX® borosilicate glass bottles and preserved with 250 μL of saturated $HgCl_2$ solution (Guo and Wong, 2015).

Nutrient concentrations were measured using an Auto Analyzer 3 (AA3) instrument (Bran + Luebbe, Germany) (Armstrong et al., 1967; Zhang et al., 1999; Dai et al., 2008) with detection limits of 0.04 μmol L^{-1} for NO_2^-, 0.1 μmol L^{-1} for $NO_2^- + NO_3^-$, 0.08 μmol L^{-1} for DIP and 0.16 μmol L^{-1} for $Si(OH)_4$ (Han et al., 2021). The analytical precisions (derived from repeated measurements of a particular aged deep seawater) were 0.5 % for $NO_2^- + NO_3^-$ (35.38 ± 0.16 μmol L^{-1}, n = 19), 0.4 % for DIP (2.66 ± 0.01 μmol L^{-1}, n = 19), and 0.2 % for $Si(OH)_4$ (128.20 ± 0.32 μmol L^{-1}, n = 19). NH_4^+ concentrations were determined using an integrated syringe-pump-based environmental-water analyzer (iSEA) based on the improved indigo phenol blue spectrophotometric method, with a detection limit of 0.15 μmol L^{-1} (Li et al., 2019). TA was measured using potentiometric titration with 0.1 mol L^{-1} hydrochloric acid, and certified reference material for carbon dioxide from Andrew G. Dickson (the Scripps Institution of Oceanography, University of California, San Diego, USA) was adopted to standardize measurements (Cai et al., 2004). Both precision and accuracy were ± 2 μmol kg^{-1}. Dissolved oxygen (DO) concentrations from discrete water samples were measured onboard using the spectrophotometric Winkler method (Labasque et al., 2004). Ca^{2+} concentrations were measured in the onshore laboratory using the EGTA titration with a Metrohm 809 TITRANDO potentiometer, which has a precision of better than ±5 μmol kg^{-1} (Cao and Dai, 2011).

2.3.2. Sampling and analysis of biological samples

Biological samples (*L. crocea*, kelp, and oyster) at the mature harvest

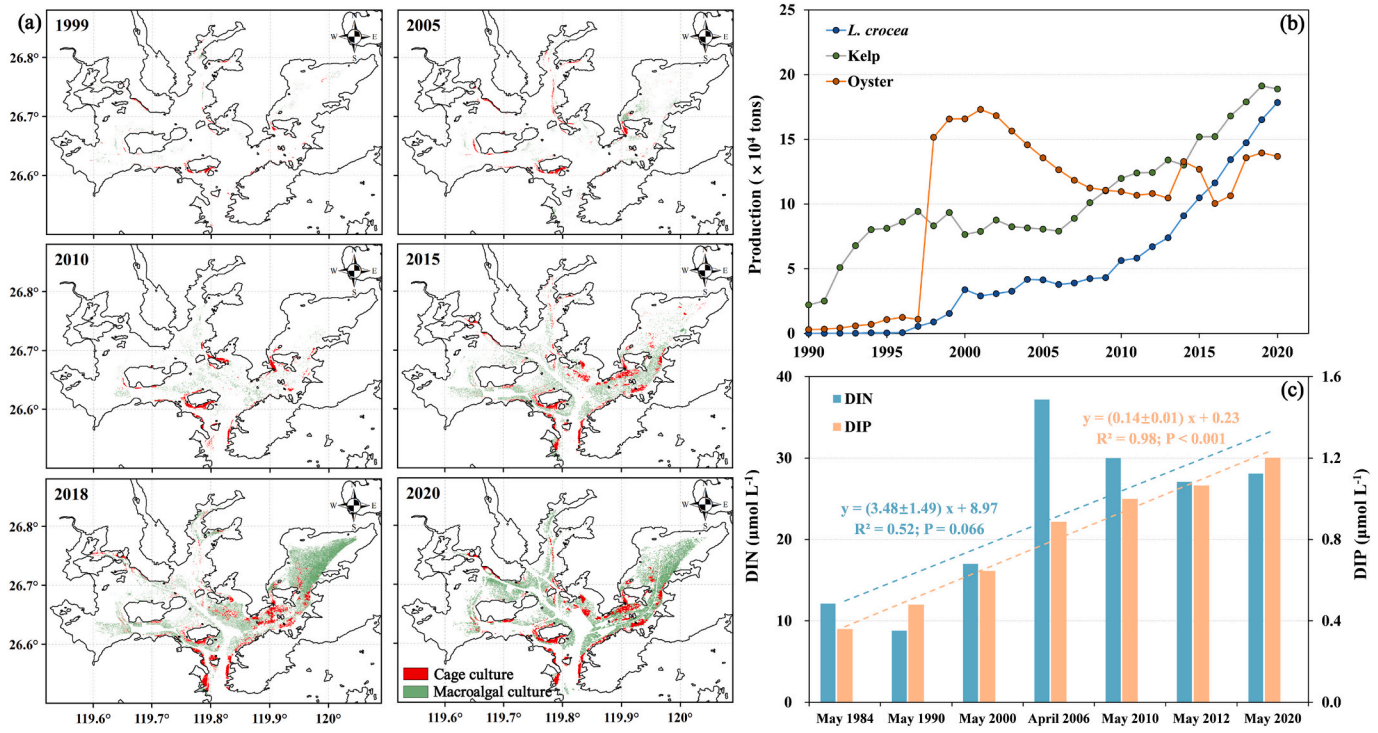

Fig. 2. (a) Classification of cage (red) and macroalgal (green) culture in Sansha Bay from 1999 to 2020. (b) Annual production trends of *L. crocea*, kelp, and oyster from 1990 to 2020 (http://tjj.ningde.gov.cn/xxgk/tjxx/tjnj/). (c) Dissolved inorganic nitrogen (DIN) and phosphorus (DIP) concentrations in Sansha Bay from 1984 to 2020. Light blue and orange dashed lines represent the linear regression lines over time for DIN and DIP, respectively; linear regression equations are also shown. (For interpretation of the references to color in this figure legend, the reader is referred to the web version of this article.)

stage were also collected and rinsed with ultrapure water for 3–4 times during the cruise. The formulated feed and trash fish feed were obtained from aquaculturists. All samples were weighed before undergoing 48 h freeze-drying process. Subsequently, the samples were reweighed to determine the percentage of dry matter. They were then ground into powder using an agate mortar for analysis. The N content was determined by wrapping 2–3 mg of sample powder in tin foil and analyzing it with an elemental analyzer (Model Vario EL cube, Elementary Co., Germany). Acetanilide and cysteine were employed as standard and quality control materials, ensuring measurement deviations stayed below 5 % (He et al., 2010). The P content was analyzed using an AA3 analyzer after ashing the samples. Approximately 2–3 mg of sample powder was mixed with 0.1 mol L^{-1} magnesium chloride solution and dried at 95 °C. It was then incinerated in a muffle furnace at 450 °C for 4 h. After adding 0.2 mol L^{-1} hydrochloric acid and heating in a water bath at 80 °C for 30 min, the sample was filtered and diluted for AA3 analysis.

2.4. Endmember mixing model

TA is assumed to be quasi-conservative in the absence of organic matter production/degradation and the exclusion of biogenic calcium carbonate production/dissolution processes (Zhai et al., 2014; Zhao et al., 2020). A two-endmember mixing model was used to construct the conservative mixing schemes between different water masses based on the TA-S diagram (Fig. S1a). Before applying this model, we considered the potential impact of submarine groundwater discharge (SGD) on TA. The endmember value of TA in SGD was approximately 1291 ± 1140 μmol kg^{-1} (red triangle in Fig. S1a) based on data from Sansha Bay during the winter of 2013 and the summer of 2014. However, our measured data do not exhibit significant deviations towards the SGD endmember. Therefore, the actual impact of SGD in this system is relatively minor, making the use of the two-endmember mixing model reasonable. Given that freshwater discharge into the bay mainly occurs via the Jiaoxi Stream, we selected station Y0, located upstream in the surveyed section of the Jiaoxi, with a salinity of 0.3 and high nutrient concentrations, as the optimal candidate for the freshwater endmember, represented by the symbol "FW". The seawater endmember is defined as East China Sea offshore water, represented by the subscript "SW". The average value of station S25, characterized by high salinity and low nutrient concentrations, was selected as the seawater endmember. A summary of the endmember values used in this study is listed in Table 1. In this context, the mixing model equations were established based on mass balance for S and the water fractions of freshwater and seawater. Subsequently, the conservative nutrient concentrations of the samples were calculated using a combination of endmember nutrient values and water fractions. The difference between the field-measured value and the predicted conservative value was denoted as Δ (ΔNutrient, i.e., ΔDIN, ΔDIP, and $\Delta Si(OH)_4$), reflecting the amount of nutrient production (positive) or removal (negative) associated with non-mixing processes (detailed in text S2). Moreover, we used Ca^{2+} as a conservative tracer (Wang et al., 2016; Su et al., 2017) to validate our endmember mixing model. The predicted Ca^{2+} values (Ca^{2+}_{pre}) are in good agreement with field-measured data (Ca^{2+}_{meas}) (Fig. S1b), which strongly supports our model predictions.

Table 1
Summary of endmember values adopted in the two-endmember mixing model.

Water masses	Salinity	DIN (μmol L^{-1})	DIP (μmol L^{-1})	$Si(OH)_4$ (μmol L^{-1})	Ca^{2+} (mmol kg^{-1})	TA (μmol kg^{-1})
Freshwater (FW)	0.3	81.34	0.976	153.52	0.27	378
Seawater (SW)	31.7 ± 0.06	13.92 ± 0.60	0.736 ± 0.022	14.75 ± 0.14	9.27 ± 0.01	2197 ± 3

2.5. Nutrient budget calculations

To assess the release, removal, and contribution of nutrients in the mariculture system within the entire Sansha Bay, we developed two nutrient budget models: one for the fish farming system (including nutrient removal by kelp and oyster) and another for the entire Sansha Bay system. The uncertainties in the budget calculations are propagated from the standard deviations of measurements of the multiple parameters in the equations (see text S5 for detailed uncertainty analysis).

2.5.1. Budgets of N and P in the mariculture system

2.5.1.1. Nutrient budgets in the fish farming system. N and P budgets of the fish farming system were established based on mass balance (Olsen and Olsen, 2008; Wang et al., 2012; Qi et al., 2019). The nutrient source of this system includes nutrient influx from feed input (F_{input}). The nutrient fate from this system includes nutrient intake by fish (F_{intake}) and the remaining particulate organic nutrient not used by fish (F_{loss}, e.g., PON-Feed, POP-Feed). The nutrient budget for this system can thus be formulated as follows:

$$dC/dt = F_{input} - F_{loss} - F_{intake} \quad (1)$$

where C is the nutrient amount. Under the assumption of a steady state ($dC/dt = 0$), Eq. (1) can be rewritten as:

$$F_{input} = F_{loss} + F_{intake} \quad (2)$$

Within the system, F_{intake} is partially used for the fish biomass ($F_{biomass}$) growth, partially excreted into the environment as dissolved inorganic nutrient ($F_{excrete}$, such as ammonia in gills or phosphate in urine), and the remaining undigested nutrients are released as particluate organic nutrient (e.g., PON-Feces, POP-Feces) through fish feces (F_{feces}), which can be represented by:

$$F_{intake} = F_{biomass} + F_{excrete} + F_{feces} \quad (3)$$

where F_{feces} and F_{loss} constitute the sources of particulate organic nutrients in the fish farming system. A small portion of these particles will be dissolved and become dissolved organic forms (DON and DOP). According to studies by Chen et al. (2003) and Sugiura et al. (2006), approximately 15 % of particulate N and P are leached out after soaking in water for several minutes or hours, with no further significant leaching thereafter. Additionally, the calculations for terms in these equations are based on parameters such as fish production (P_{fish}), feed conversion rate (R_{conv}), feed loss rate (R_{loss}), assimilation efficiency (R_{assim}), N and P contents (C_{NP}), and dry matter ratio (R_{dry}). Detailed calculation processes and parameter values are provided in text S3 and Table S2.

2.5.1.2. Nutrient removal by kelp and oyster in the mariculture system. Under the assumption of negligible nutrient release during kelp and oyster cultivation, their harvest can effectively remove N and P from the environment. For kelp, the amount removed ($F_{removal,kelp}$) can be calculated as:

$$F_{removal,kelp} = P_{kelp} \times R_{dry,kelp} \times C_{NP,kelp} \quad (4)$$

where P_{kelp} is kelp production; $R_{dry,kelp}$ is the percentage of dry matter in kelp; and $C_{NP,kelp}$ is the N and P content in kelp.

For oysters, the amount removed ($F_{removal,oyster}$) includes both the shell and soft tissue harvesting, which can be calculated as:

$$F_{removal,oyster} = P_{oyster} \times R_{dry,shell} \times C_{NP,shell} + P_{oyster} \times R_{dry,tissue} \times C_{NP,tissue} \quad (5)$$

where P_{oyster} is oyster production; $R_{dry,shell}$ and $R_{dry,tissue}$ are the dry weight percentages of oyster shell and soft tissue; $C_{NP,shell}$ and $C_{NP,tissue}$ are the N and P contents of oyster shell and soft tissue, respectively. The data involved in the calculations are summarized in Table S2.

2.5.2. Budgets of DIN and DIP in Sansha Bay system

To assess the impact of DIN and DIP released from the fish farming system on the entire Sansha Bay system, we treated Sansha Bay as a single box. Nutrient fluxes from river input and exchange with offshore coastal waters were calculated based on the Land-Ocean Interactions in the Coastal Zone (LOICZ) model (Gordon et al., 1996; Han et al., 2021). The exchange flow discharge (V_{ex}) between the bay and offshore coastal waters was estimated based on water and salt mass balance. Subsequently, DIN and DIP fluxes (F_{DIN} and F_{DIP}) were calculated using water discharge and corresponding nutrient concentrations in the model. Detailed calculation information is provided in text S4.

3. Results and discussions

3.1. Nutrient and physicochemical parameters distributions in Sansha Bay

During spring in Sansha Bay, the temperature exhibited spatial variability. It reached a maximum of 22.5 °C in Baima Harbor, located upstream of the bay, while a lower temperature (~21.9 °C) was observed near the Dongchong Channel at the mouth of Sansha Bay (Fig. 3a). The salinity increased gradually from the inner bay to the mouth, ranging from 0.3 in the Jiaoxi Stream to 31.7 in the Dongchong Channel (Fig. 3b). Therefore, Sansha Bay is characterized by lower temperature and higher salinity at its mouth compared to the upstream area due to the influence of river runoff from the northwest of the bay and coastal ECS waters.

Nutrient concentrations generally decreased from the inner to outer portion of the bay. The highest $NO_3^- + NO_2^-$ (76.1 μmol L^{-1}) and $Si(OH)_4$ (153.5 μmol L^{-1}) concentrations were found in the Jiaoxi Stream, and they decreased linearly with increasing salinity (Fig. 3e and f). The highest DIP and NH_4^+ concentrations were not observed in the Jiaoxi Stream, but rather in waters near Sandu Island (stations S1, S2, S6, and S26) and Guanjingyang (station S14) (Fig. 3g and h), which may result from the release of fish feed (Fig. 3i). The DO distribution showed higher concentrations in the inner bay and lower concentrations near the bay mouth (Fig. 3d). The higher DO concentrations (6.25–6.75 mg L^{-1}) near Sandu Island correspond to areas with higher Chl-*a* levels, which may be attributed to increased photosynthesis in the region. However, overall Chl-*a* concentrations were low (<1 μg L^{-1}) and uniform throughout the study area (Fig. 3c), indicating relatively low phytoplankton productivity. The primary reason for this characteristic is nutrient competition (Huang et al., 2017), allelopathy (Cheng and Cheng, 2015), and shading effect (Fong and Zedler, 1993) caused by macroalgal cultivation, which inhibit the growth of phytoplankton (Xie et al., 2021).

The water was well-mixed throughout the water column, with only weak stratification in the upstream area, as shown in Fig. 4. Overall, nutrient concentrations at different depths followed a similar pattern to their distribution in the surface layer, showing zonal variation from the inner to the outer portion of the bay. The $NO_3^- + NO_2^-$ concentrations decreased from 62.4–76.1 μmol L^{-1} at the upstream to 9.3–11.9 μmol L^{-1} at the Dongchong Channel. $Si(OH)_4$ concentrations exhibited a similar spatial distribution, gradually decreasing seaward. Lower concentrations were also observed near the Dongchong Channel, ranging from 0.71 to 0.92 μmol L^{-1} for DIP, and 3.99 to 5.46 μmol L^{-1} for NH_4^+, while the values were higher in Baima Harbor (Station SX01). Additionally, higher DIP and NH_4^+ concentrations observed at station S14 were associated with a minimal DO concentration (~5.6 mg L^{-1}), which may result from organic matter remineralization. The Chl-*a* also exhibited relatively low levels at different depths (Fig. 4c) due to the influence of macroalgal cultivation.

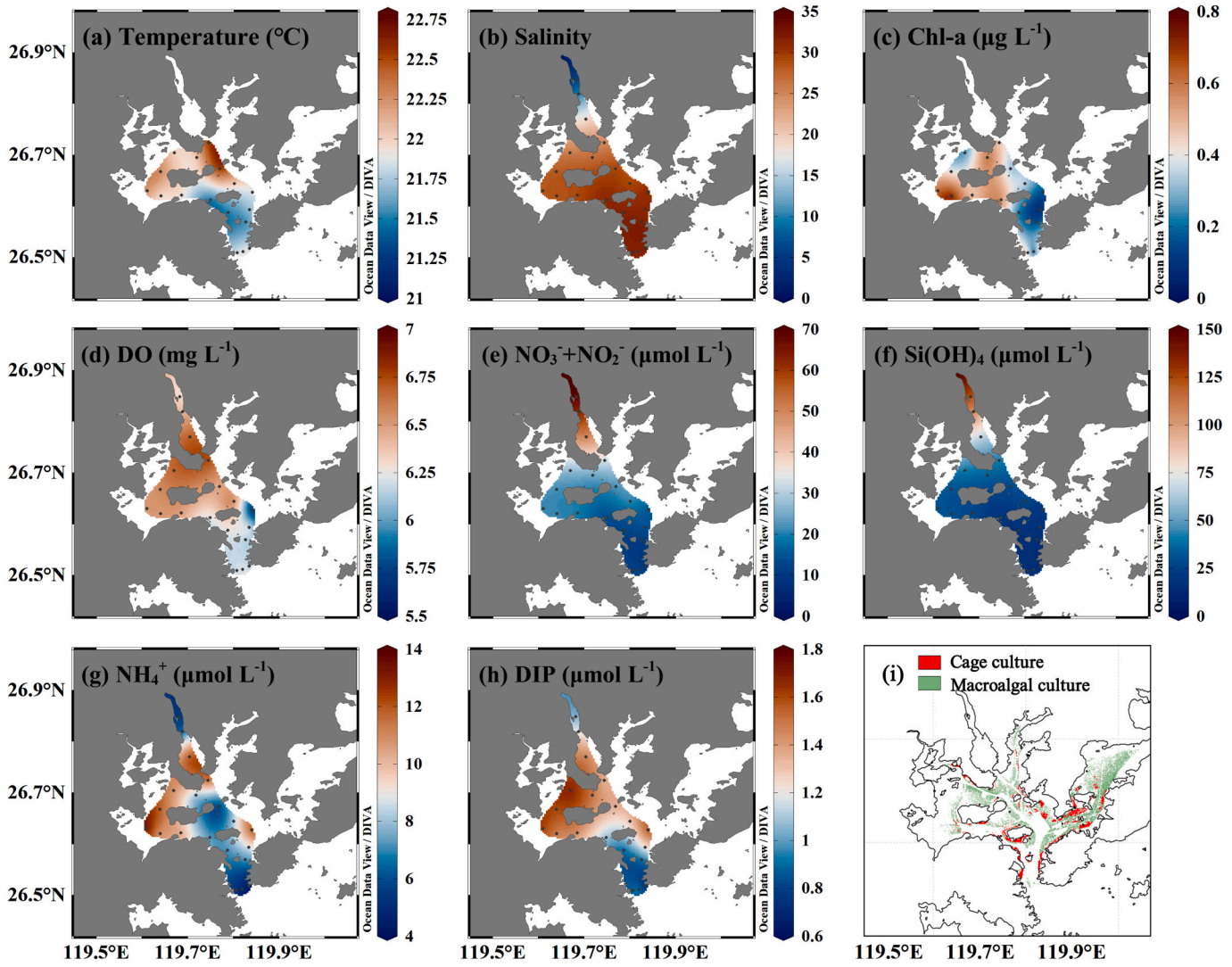

Fig. 3. Distributions of temperature, salinity, chlorophyll-*a* (Chl-*a*), dissolved oxygen (DO), nitrate + nitrite (NO_3^- + NO_2^-), silicate ($Si(OH)_4$), ammonium (NH_4^+), and dissolved inorganic phosphorus (DIP) in surface waters of Sansha Bay (a–h). Distributions of macroalgal and cage culture in surface waters (i) are shown in green and red, respectively. (For interpretation of the references to color in this figure legend, the reader is referred to the web version of this article.)

3.2. Nutrient changes due to biogeochemical processes and nutrient stoichiometric ratios

The DIN concentration gradually decreased with increasing salinity and exhibited obvious addition within the bay, attaining 6.9 ± 4.1 μmol L^{-1} (34.5 % ± 16.3 %) throughout the bay area (Fig. 5a). However, the behavior of DIP differed in that the variation in DIP concentrations was more complex, with a S value of 25 serving as the boundary. DIP concentration gradually increased at S < 25, while they decreased when S exceeded 25. In Sansha Bay, we observed a DIP addition of 0.45 ± 0.29 μmol L^{-1} (58.8 % ± 37.0 %), with a maximum addition of 1.19 μmol L^{-1} in the mariculture zone. This pattern was likely induced by a buffering mechanism of DIP (Froelich, 1988), and/or variation in feed inputs in different zones (Fig. 5b). However, the DIP buffering mechanism generally operates in low-salinity (S < 15) estuarine regions (Froelich, 1988). Our observations covered only a few stations with S below 15, indicating that the overall impact of the buffering mechanism was minimal compared to that of mariculture. Additionally, we observed conservative behavior in $Si(OH)_4$. Although diatoms were dominant in this bay during spring, their abundance was relatively low, corresponding to low Chl-*a* concentrations (Fig. 3c). As a result, individual stations deviated slightly from the conservative mixing line at salinity below 25 (Fig. 5c).

Overall, distinct DIN:DIP ratios associated with different water masses resulted in variable effects on nutrient stoichiometry. The significant inflow of DIN from the Jiaoxi Stream caused the brackish water to exhibit a high DIN:DIP ratio (Fig. 6a). Beyond that, the relationship between DIN and DIP in the water column was quite homogeneous, with the ratio slightly higher than the Redfield ratio (Redfield et al., 1963), which is consistent with previous observations in other mariculture waters in China (Bouwman et al., 2013; Qi et al., 2019). The $Si(OH)_4$: DIN ratio, however, exhibited different characteristics: it was significantly higher than the diatom absorption ratio of 1:1 in the brackish water (Brzezinski, 1985; Martin-Jézéquel et al., 2003). This is likely attributable to the weathering of volcanic rock, which is dominant in Ningde and results in relatively high silicate concentrations. In regions excluding the brackish water, the overall $Si(OH)_4$:DIN ratio approximated the line of 1:1 (Fig. 6b).

Results from the endmember mixing model showed significant DIN and DIP additions (positive values) at most stations. Specifically, we calculated ΔDIN and ΔDIP to be 6.9 ± 4.1 μmol L^{-1} and 0.45 ± 0.29 μmol L^{-1}, respectively, with a ratio of approximately 15.33. This ratio was comparable to that observed in specific mariculture zone (the red star stations in Fig. 1). Therefore, the ΔDIN:ΔDIP ratio was primarily

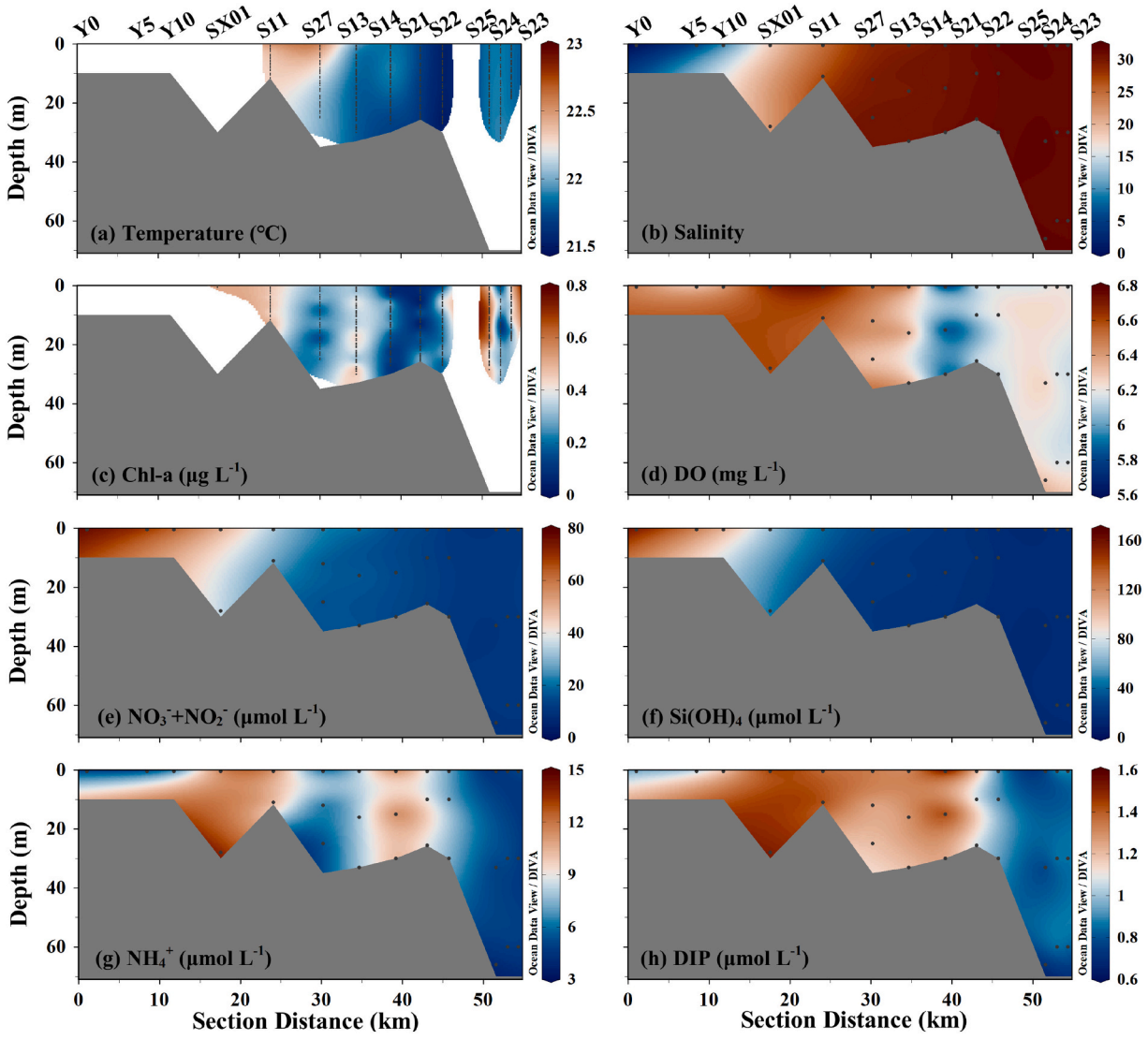

Fig. 4. Distributions of temperature, salinity, chlorophyll-*a* (Chl-*a*), dissolved oxygen (DO), nitrate + nitrite (NO_3^- + NO_2^-), silicate ($Si(OH)_4$), ammonium (NH_4^+), and dissolved inorganic phosphorus (DIP) along the main transect of Sansha Bay (a–h) from the Jiaoxi Stream (0 km) to the Dongchong Channel. Black circles within the transect indicate stations.

influenced by mariculture activities and may also be related to organic matter remineralization. Previous study indicated that processes such as the preferential remineralization of phosphorus in the water column can partially reduce the N:P ratio in the water (Bu et al., 2024). Moreover, there was no obvious pattern for the $\Delta Si(OH)_4$:ΔDIN ratio because $Si(OH)_4$ is basically conservative in Sansha Bay.

3.3. Nutrient budget in the mariculture system

3.3.1. Nutrient release from the fish farming system

In spring 2020, the production of *L. crocea* in Sansha Bay was 4.46×10^4 tons (dry matter: ~31.88 %). Among this, 80 % of the production (3.57×10^4 tons) was fed by trash fish feed, while the remaining 20 % of the production (8.92×10^3 tons) was fed by formulated feed. Based on the feed conversion rate, the feed input in spring included about 2.41×10^5 tons (dry matter: ~27.68 %) of fresh trash fish feed and 1.36×10^4 tons (dry matter: 100 %) of formulated feed. To evaluate the N and P amounts of feed input, we also measured the N and P contents in the trash fish and formulated feeds, which were 10.03 ± 0.06 %, 7.82 ± 0.07 % for N, and 1.91 ± 0.09 %, 1.59 ± 0.05 % for P, respectively (Table S2). Therefore, the feed inputs were 6725 ± 361 tons of N and 1281 ± 91 tons of P in the trash fish feed system, and 1064 ± 11 tons of N and 216 ± 7 tons of P in the formulated feed system (Fig. 7).

In the trash fish feed system, based on the determined N and P contents in fish (12.17 ± 0.56 % for N, 1.17 ± 0.002 % for P), about 1384 ± 64 tons of N and 133 ± 0.23 tons of P were incorporated into fish tissues, corresponding to only 20.6 ± 1.5 % of N and 10.4 ± 0.7 % of P from feed input, respectively. The remaining nutrients were released and lost to seawater or sediment (Fig. 7a and b). Specifically, in the N budget model, N excretion in DIN form totaled 3589 ± 316 tons, representing 53.4 ± 5.5 % of the feed input. In PON form, which includes feed loss and fecal matter, N release amounted to 1489 ± 408 tons, accounting for 22.1 ± 6.2 %. Additionally, about 263 ± 72 tons of the PON waste was subsequently dissolved into DON (Fig. 7a). In the P budget model, however, ca. 615 ± 88 tons (48.0 ± 7.7 %) and 424 ± 46 tons (33.1 ± 4.3 %) of P were lost as POP and DIP, respectively (Fig. 7b). Similarly, in the formulated feed system, approximately 32.5 ± 1.5 % of N and 15.4 ± 0.5 % of P in feed were absorbed and utilized for incorporation in fish biomass (Fig. 7c and d), a proportion higher than that calculated in the trash fish feed system. In the N budget model, about half of N (49.1 ± 2.2 %) was lost as DIN (Fig. 7c). While, 44.2 ± 3.8 % of P was deposited as particulates in the P budget model (Fig. 7d).

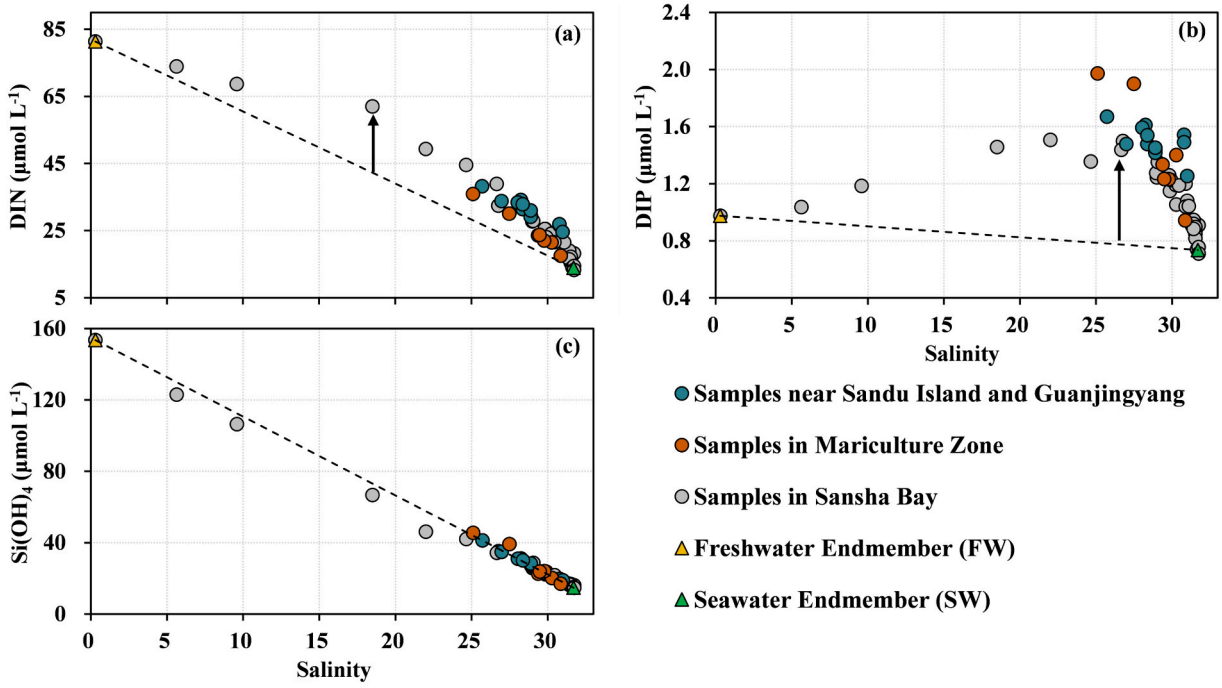

Fig. 5. Relationships between nutrient concentrations and salinity in Sansha Bay in May 2020. Dark green, red, and gray circles indicate stations near Sandu Island (S1, S2, S6 and S26) and Guanjingyang (S14), mariculture zone, and other stations in Sansha Bay. Freshwater and seawater endmembers are shown by yellow and green triangles, respectively. Black dashed lines represent the conservative mixing line, with black arrows indicating the addition of dissolved inorganic nitrogen (DIN) and phosphorus (DIP) based on the conservative mixing lines. (For interpretation of the references to color in this figure legend, the reader is referred to the web version of this article.)

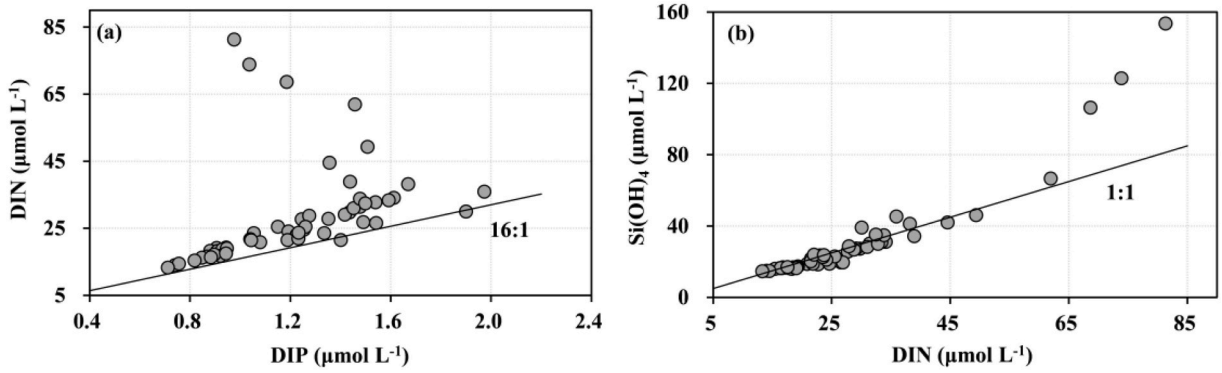

Fig. 6. (a) Relationships between dissolved inorganic nitrogen and phosphorus (DIN and DIP), (b) silicate ($Si(OH)_4$) and DIN in Sansha Bay. The solid lines represent a DIN to DIP ratio of 16:1 and a $Si(OH)_4$ to DIN ratio of 1:1.

Additionally, the released DIN:DIP ratios showed inconsistencies. Molar DIN:DIP ratios were ~18.74 and ~16.28 in the trash fish feed and formulated feed systems, respectively, which might explain the variable ΔDIN:ΔDIP ratios in the waters.

In summary, in both feeding systems co-fed with trash fish and formulated feeds, the total feed input of N and P was 7789 ± 361 tons and 1497 ± 91 tons during spring, respectively. Among these, only 1730 ± 66 tons (22.2 ± 1.3 %) of N and 166 ± 0.23 tons (11.1 ± 0.7 %) of P were assimilated by cultured fish, with the remaining nutrients being released into the environment in different forms (data listed in Table S3). Of these released nutrients, approximately 4111 ± 317 tons (52.8 ± 4.7 %) of DIN and 495 ± 46 tons (33.0 ± 3.7 %) of DIP released into the water, as well as 1655 ± 409 tons (21.2 ± 5.3 %) of PON and 711 ± 88 tons (47.5 ± 6.6 %) of POP settling to the bottom (Fig. 8). These results indicate that the retention rate of N in fish biomass was higher compared to P, and the proportion of N excreted by fish was lower than that of P. Additionally, the majority of N waste generated by the fish farming system was excreted as DIN, whereas the majority of P waste settled as POP.

3.3.2. *Model sensitivity analysis*

The accuracy of input data is crucial for model predictions. The feed loss rates and assimilation efficiencies of different feeds are relatively uncertain. Therefore, we conducted a sensitivity analysis of the model, using the N budget in the trash fish feed system as an example. Our budget model showed that N and P released from the system fed by trash fish feed was much greater than that from the system fed by formulated feed due to the higher feed loss rate in trash fish feed. Specifically, Fig. S2a demonstrated a progressive rise in the release of DIN and loss of PON-Feed with an increasing percentage of trash fish feed, while DON and PON-Feces were less variable. Therefore, formulated feed with varying particle sizes may be used for different fish sizes compared to the

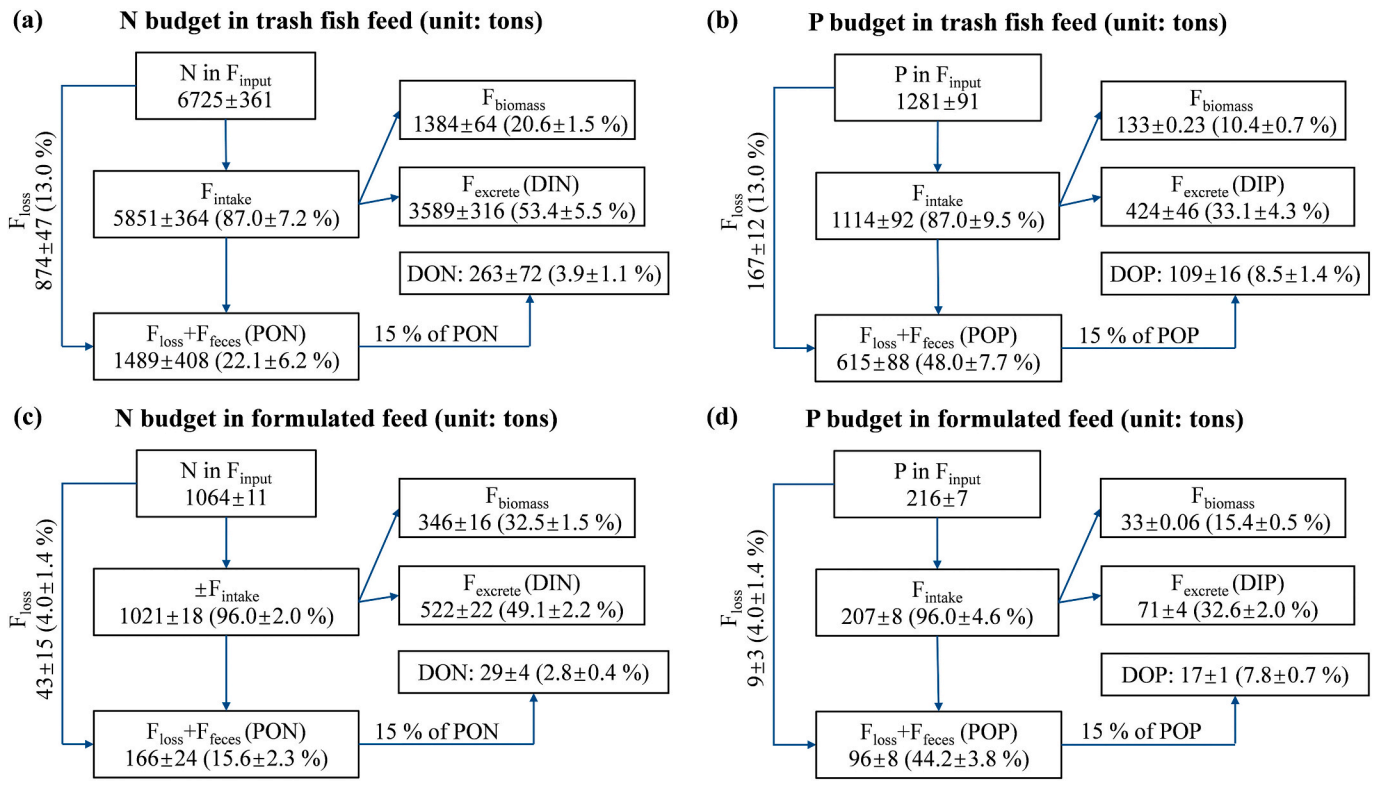

Fig. 7. Nitrogen (N; (a) and (c)) and phosphorus (P; (b) and (d)) budgets for the fish farming system using trash fish and formulated feeds in Sansha Bay during spring. Percentage values represent the proportion of each component relative to N and P from feed input. DIN and DIP: dissolved inorganic nitrogen and phosphorus, respectively; DON and DOP: dissolved organic nitrogen and phosphorus, respectively; PON and POP: particulate organic nitrogen and phosphorus, respectively. Abbreviations for fluxes (F) refer to Section 2.5.1.

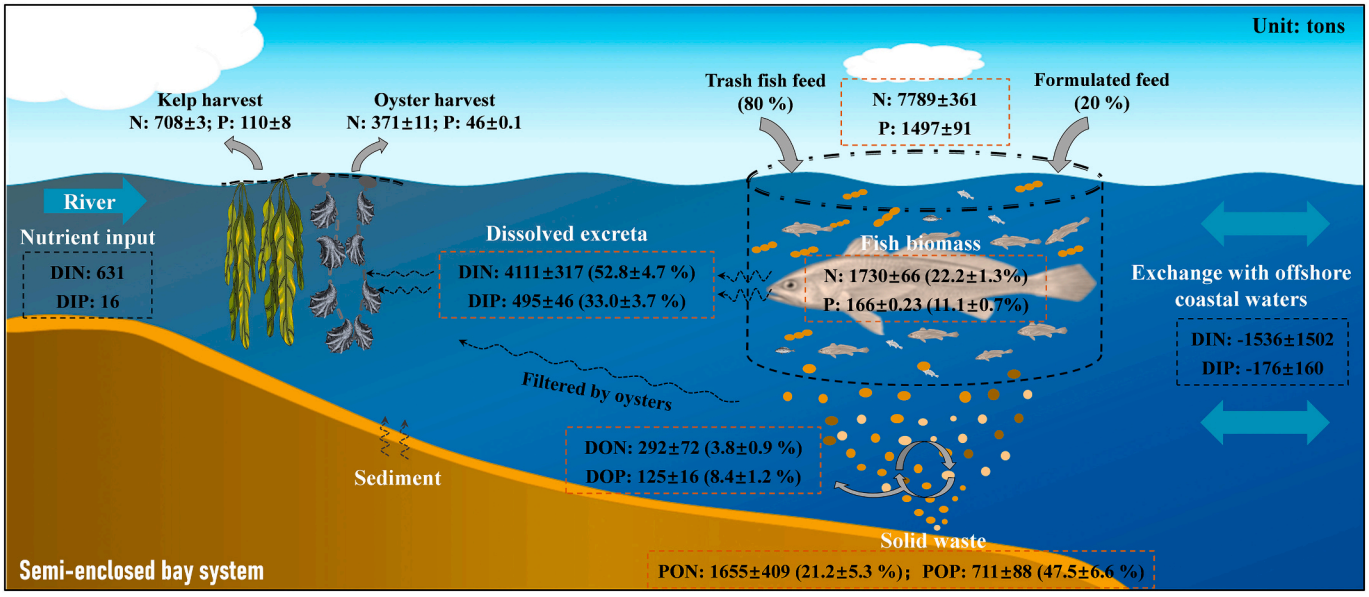

Fig. 8. Conceptual diagram illustrating the nutrient transformations of different species resulting from mariculture in the semi-enclosed bay system, which was influenced by riverine input and offshore coastal water exchange. The units in the figure are given in tons. Negative values indicate nutrient output. Nutrient abbreviations as in Fig. 7.

trash fish feed, which can reduce feed loss during farming. In addition, N and P retention rates of trash fish feed were lower than those of formulated feed. According to Verdegem et al. (1999), the higher feed protein content, typically found in trash fish feed, leads to a greater proportion of N waste being excreted. Moreover, the lower nutritional value and digestibility of trash fish feed may also explain its lower N retention rate (Hasan et al., 2016; Qi et al., 2019). The impacts of different feed losses and assimilation efficiencies were shown in Fig. S2b and c. In the above calculations for the trash fish feed system, a 13 % feed loss value and 85 % N assimilation efficiency were used. The

percentage of DIN excretion decreased as feed loss increased, and the percentage of PON-Feed increased in a comparable manner (Fig. S2b). In contrast, a rise in the percentage of DIN and a decline in the percentage of PON-Fecal were found with an increase in assimilation efficiency (Fig. S2c). The results indicated that changes in assimilation efficiency, for example, from 80 % to 90 %, caused model uncertainties of <10 %. Therefore, minor changes in feed loss and assimilation efficiency are unlikely to result in significant deviations in model predictions.

3.3.3. Nutrient removal by macroalgae and oyster harvesting

As previously mentioned, based on the feed input and fish harvesting, the N and P released by fish farming were 6059 ± 367 tons and 1331 ± 91 tons, respectively. To better evaluate and further understand the nutrient removal in the mariculture system, the contents in the kelp, oyster soft tissue, and oyster shell were determined: 2.25 ± 0.01 %, 8.07 ± 0.10 %, 0.16 ± 0.01 % for N, and 0.35 ± 0.027 %, 0.56 ± 0.002 %, 0.044 ± 0.000 % for P, respectively (Table S2). The results showed that kelp harvesting in Sansha Bay resulted in the removal of 708 ± 3 tons of N and 110 ± 8 tons of P, respectively. In the case of oyster harvesting, it removed 371 ± 11 tons of N and 46 ± 0.1 tons of P (Fig. 8). Therefore, the co-culture strategy removed a total of 1079 ± 11 tons of N and 156 ± 8 tons of P. As a result, the total releases of N and P from the mariculture system in spring were 4980 ± 367 tons and 1175 ± 92 tons, respectively. Results showed that the amount of N and P released from feed was much higher than that removed by the combined harvest of fish, macroalgae and oyster.

3.4. Nutrient budget in Sansha Bay during spring

To further clarify the nutrient contribution of the fish farming system to the whole water in Sansha Bay, we estimated the DIN and DIP fluxes contributed by river discharge and exchange with offshore coastal waters, as detailed in text S4. The river discharge (71.3 $m^3\ s^{-1}$, data from Nengwang Chen, Xiamen University) and measured nutrient concentrations in May were used for estimating fluxes of river input and exchange with offshore coastal waters. Results showed that the residual flow and the exchange flow discharge between the bay and offshore coastal waters were −71.3 $m^3\ s^{-1}$ (negative values indicating outflow) and 720.1 ± 676.8 $m^3\ s^{-1}$, respectively (Table 2), which was also comparable with previous data (~479.5 $m^3\ s^{-1}$, unpublished data from Zhaozhang Chen, Xiamen University). Assuming that the data measured in May reflected spring characteristics, the DIN and DIP fluxes from the river over the spring season (90 days) were 631 and 17 tons, respectively, while nutrient fluxes from the bay to offshore coastal waters were 1536 ± 1502 tons for DIN and 176 ± 160 tons for DIP (Fig. 8). As a result, without considering the contributions from other sources such as atmospheric deposition, SGD, and sediment processes, the amount of dissolved inorganic nutrients (DIN: 4111 ± 317 tons; DIP: 495 ± 46 tons) released by the fish farming system was much higher than that from river input, making them the primary source of nutrients in Sansha Bay. And DIN and DIP transported from Sansha Bay through the Dongchong Channel to coastal ocean account for approximately 32.4 % and 34.4 % of the river inputs and feed release inputs, respectively.

Table 2
Summary of salinity (S), dissolved inorganic nitrogen (DIN) and phosphorus (DIP) concentrations (μmol L^{-1}), water discharge (V, $m^3\ s^{-1}$), and calculated nutrient fluxes (F_{DIN} and F_{DIP}, tons) in the mass balance model.

Salinity	S_{riv}	$S_{sys} \pm \sigma_{sys}$	$S_{oce} \pm \sigma_{oce}$	$S_{res} \pm u_{res}$
	0.3	29.1 ± 2.7	32.1 ± 0.8	30.6 ± 1.4
DIN (μmol L^{-1})	DIN_{riv}	$DIN_{sys} \pm \sigma_{DINsys}$	$DIN_{oce} \pm \sigma_{DINoce}$	$DIN_{res} \pm u_{DINres}$
	81.3	27.5 ± 9.0	9.7 ± 2.8	18.6 ± 4.7
DIP (μmol L^{-1})	DIP_{riv}	$DIP_{sys} \pm \sigma_{DIPsys}$	$DIP_{oce} \pm \sigma_{DIPoce}$	$DIP_{res} \pm u_{DIPres}$
	0.98	1.29 ± 0.27	0.36 ± 0.10	0.83 ± 0.14
V ($m^3\ s^{-1}$)	V_{riv}	$V_{ex} \pm u_{ex}$		V_{res}
	71.3	720.1 ± 676.8		−71.3
F_{DIN} (tons)	F_{DINriv}	$F_{DINex} \pm u_{FDINex}$		$F_{DINres} \pm u_{FDINres}$
	631	−1392 ± 1501		−144 ± 36
F_{DIP} (tons)	F_{DIPriv}	$F_{DIPex} \pm u_{FDIPex}$		$F_{DIPres} \pm u_{FDIPres}$
	17	−161 ± 160		−14 ± 2

Note: S_{riv} represents the salinity of station Y0 in the Jiaoxi Stream; S_{sys} represents the average salinity in the bay, excluding stations Y0, Y5, Y10 in the stream and S23, S24, S25 at the bay mouth; S_{oce} represents the salinity of four stations (LJ21, LJ22, ND41, and ND42) in offshore coastal waters; S_{res} represents the salinity of the residual flow; V_{riv}, V_{res} and V_{ex} represent the river discharge, residual flow discharge from the bay to offshore coastal waters and exchange flow discharge between the bay and offshore coastal waters, respectively; σ represents the standard deviation, and u represents the uncertainty associated with each variable. Negative values indicate nutrient output.

Based on historical literature on atmospheric deposition of nutrients, the total atmospheric deposition flux of DIN at Shengsi Island in the East China Sea was 0.96 g N $m^{-2}\ yr^{-1}$ (Zhang et al., 2007). In Lianjiang during summer (July), the total atmospheric deposition fluxes of DIN and DIP were 5920 mol d^{-1} and 10.1 mol d^{-1}, respectively, based on a study area of 53 km^2 (Peng et al., 2021). The wet deposition flux of DIN in the coastal area near Fuzhou was 14.23 kg N $ha^{-1}\ yr^{-1}$ (Luo et al., 2014). Due to the lack of direct monitoring data in Sansha Bay, this study used the average data from these regions as a substitute (DIN: 0.98 ± 0.35 g N $m^{-2}\ yr^{-1}$; DIP: 2.16 mg P $m^{-2}\ yr^{-1}$) to estimate the total atmospheric deposition inputs of DIN and DIP, which are 163 ± 58 tons and 0.36 tons in spring (90 days), respectively. These values are significantly lower than the river input and feed release from mariculture system during spring.

In addition, SGD acts as an important pathway for terrestrially derived materials into the coastal ocean, and its impact on nutrient fluxes cannot be ignored (Kim et al., 2011; Wang et al., 2018). Wang et al. (2018) observed substantial seasonal variations in nutrient fluxes through SGD in Sansha Bay. Specifically, the SGD-associated nutrient flux was (1.65–1.76) × 10^6 mol d^{-1} in winter and (1.62–2.28) × 10^7 mol d^{-1} in summer for DIN, and (0.05–2.32) × 10^4 mol d^{-1} in winter and (0–2.17) × 10^5 mol d^{-1} in summer for DIP. Therefore, the estimated nutrient fluxes from SGD ranged from 2142 tons in winter to 24,570 tons in summer for DIN, and from 33 tons in winter to 301 tons in summer for DIP based on the average values of two seasons. Compared to nutrient releases from spring mariculture, the winter DIN flux from SGD was lower, while the summer DIN flux was notably higher. In contrast, both winter and summer DIP fluxes were lower than those from spring mariculture. This indicates that SGD-associated nutrients have a potential impact on the system, which should not be ignored. However, it is worth noting that the DIN:DIP ratio in SGD exceeded 70 (Wang et al., 2018), and our measured data during spring do not reveal a significant increase in the ratio, indicating that SGD has not yet directly affected the nutrient composition of this bay. Additionally, the river discharge observed in this study during spring was an order of magnitude lower than that observed in summer, and comparable to that in winter (Wang et al., 2018), suggesting that seasonal variations in river discharge may also contribute to the differences in nutrient fluxes in SGD. Therefore, although SGD-associated nutrient fluxes are substantial, the direct release of nutrients from the mariculture system has a more pronounced effect on eutrophication and the ecosystem of the bay.

4. Conclusions and perspectives

The spatial variability of nutrients in Sansha Bay was mainly controlled by the mixing of water masses between the riverine water and seawater, as well as the effects of the mariculture system. Based on the endmember mixing model, we estimated that the additions of DIN and DIP during spring were approximately 6.9 ± 4.1 μmol L^{-1} and 0.45 ± 0.29 μmol L^{-1}, respectively. When using a mixture of formulated feed and trash fish feed at a 2:8 ratio, it was observed that approximately 52.8 ± 4.7 % of DIN and 33.0 ± 3.7 % of DIP from the feeds were released into the surrounding waters, significantly surpassing the river input and

exchange with offshore coastal waters. The economic preference for lower-cost trash fish feed, despite its higher environmental costs (a 77.4 % increase in trash fish feed required to produce one ton of fish compared to the formulated feed due to higher feed conversion rates), underscores the urgent need for sustainable feed strategies. Enhancing feed conversion rates, optimizing feed compositions, and strategically reducing production costs are critical steps towards mitigating environmental impacts while maintaining economic viability in the fish farming system.

However, integrated approaches such as the cultivation of macroalgae and bivalves offer promising solutions for nutrient removal. These species can effectively assimilate nutrients from mariculture waste, thereby mitigating environmental impacts. Nevertheless, the optimal deployment of such biofiltration methods requires further investigation and planning. In summary, addressing the dual challenges of economic feasibility and environmental sustainability in the mariculture system requires comprehensive monitoring and corresponding management practices. One initiative is the Ningde municipal government's effort to remove mariculture activities from the inner bay to the outer bay. However, it remains uncertain whether these measures will exacerbate HABs outbreaks outside the bay and reach a tipping point. Therefore, by focusing on long-term studies of nutrient dynamics, water quality responses, and ecological indicators, we can reduce the risks associated with nutrient pollution and ecosystem degradation, thereby guiding effective policies and practices in Sansha Bay and similar coastal environments.

CRediT authorship contribution statement

Yanmin Wang: Writing – original draft, Visualization, Validation, Methodology, Investigation, Formal analysis. **Xianghui Guo:** Writing – review & editing, Validation, Conceptualization. **Guizhi Wang:** Writing – review & editing, Validation, Conceptualization. **Lifang Wang:** Resources, Investigation, Data curation. **Tao Huang:** Resources, Investigation, Data curation. **Yan Li:** Resources, Investigation. **Zhe Wang:** Resources, Project administration. **Minhan Dai:** Writing – review & editing, Supervision, Funding acquisition, Conceptualization.

Declaration of competing interest

The authors declare that they have no known competing financial interests or personal relationships that could have appeared to influence the work reported in this paper.

Data availability

Data will be made available on request.

Acknowledgement

We thank the captain, crew, and scientific staff of the R/V *Funing 11* for their cooperation during the cruise, Kunning Lin for sample collection and ammonium analysis; Aiqin Han for assistance in sample collection, Yi Xu for the collection of biological samples, Nengwang Chen and Xuwen Fang for providing the YSI and river discharge data, Junhui Chen for guidance in sample analysis, Haixia Guo for processing the remote sensing data, Yanping Xu and Feifei Meng for their logistical support. This work was supported by the National Natural Science Foundation of China (NSFC #42188102) and by the Research Grants Council of the Hong Kong Special Administrative Region, China (Project Reference Number: AoE/P-601/23-N).

Appendix A. Supplementary data

Supplementary data to this article can be found online at https://doi.org/10.1016/j.marpolbul.2024.117085.

References

Anderson, D.M., Glibert, P.M., Burkholder, J.M., 2002. Harmful algal blooms and eutrophication: nutrient sources, composition, and consequences. Estuaries 25, 704–726. https://doi.org/10.1007/BF02804901.

Armstrong, F.A.J., Stearns, C.R., Strickland, J.D.H., 1967. The measurement of upwelling and subsequent biological process by means of the Technicon Autoanalyzer and associated equipment. Deep-Sea Res. Oceanogr. Abstr. 14, 381–389. https://doi.org/10.1016/0011-7471(67)90082-4.

Bouwman, L., Beusen, A., Glibert, P.M., Overbeek, C., Pawlowski, M., Herrera, J., Mulsow, S., Yu, R., Zhou, M., 2013. Mariculture: significant and expanding cause of coastal nutrient enrichment. Environ. Res. Lett. 8, 044026. https://doi.org/10.1088/1748-9326/8/4/044026.

Breitburg, D., Levin, L.A., Oschlies, A., Gregoire, M., Chavez, F.P., Conley, D.J., Garcon, V., Gilbert, D., Gutierrez, D., Isensee, K., Jacinto, G.S., Limburg, K.E., Montes, I., Naqvi, S.W.A., Pitcher, G.C., Rabalais, N.N., Roman, M.R., Rose, K.A., Seibel, B.A., Telszewski, M., Yasuhara, M., Zhang, J., 2018. Declining oxygen in the global ocean and coastal waters. Science 359. https://doi.org/10.1126/science.aam7240.

Brzezinski, M.A., 1985. The Si:C:N ratio of marine diatoms: interspecific variability and the effect of some environmental variables. J. Phycol. 21, 347–357. https://doi.org/10.1111/j.0022-3646.1985.00347.x.

Bu, D., Zhu, Q., Li, J., Huang, J., Zhuang, Y., Yang, W., Qi, D., 2024. Mariculture may intensify eutrophication but lower N/P ratios: a case study based on nutrients and dual nitrate isotope measurements in Sansha Bay, southeastern China. Front. Mar. Sci. 11. https://doi.org/10.3389/fmars.2024.1351657.

Cai, W., Dai, M., Wang, Y., Zhai, W., Huang, T., Chen, S., Zhang, F., Chen, Z., Wang, Z., 2004. The biogeochemistry of inorganic carbon and nutrients in the Pearl River estuary and the adjacent Northern South China Sea. Cont. Shelf Res. 24, 1301–1319. https://doi.org/10.1016/j.csr.2004.04.005.

Campanati, C., Willer, D., Schubert, J., Aldridge, D.C., 2021. Sustainable intensification of aquaculture through nutrient recycling and circular economies: more fish, less waste, blue growth. Rev. Fish. Sci. Aquacult. 30, 143–169. https://doi.org/10.1080/23308249.2021.1897520.

Cao, L., Naylor, R., Henriksson, P., Leadbitter, D., Metian, M., Troell, M., Zhang, W., 2015. China's aquaculture and the world's wild fisheries. Science 347, 133–135. https://doi.org/10.1126/science.1260149.

Cao, Z., Dai, M., 2011. Shallow-depth $CaCO_3$ dissolution: evidence from excess calcium in the South China Sea and its export to the Pacific Ocean. Glob. Biogeochem. Cycles 25. https://doi.org/10.1029/2009gb003690.

Carboni, S., Clegg, S.H., Hughes, A.D., 2016. The use of biorefinery by-products and natural detritus as feed sources for oysters (*Crassostrea gigas*) juveniles. Aquaculture 464, 392–398. https://doi.org/10.1016/j.aquaculture.2016.07.021.

Chen, C.L., Qiu, G.H., 2014. The long and bumpy journey: Taiwans aquaculture development and management. Mar. Policy 48, 152–161. https://doi.org/10.1016/j.marpol.2014.03.026.

Chen, Y.S., Beveridge, M., Telfer, T.C., Roy, W.J., 2003. Nutrient leaching and settling rate characteristics of the faeces of Atlantic salmon (*Salmo salar* L.) and the implications for modelling of solid waste dispersion. J. Appl. Ichthyol. 19, 114–117. https://doi.org/10.1046/j.1439-0426.2003.00449.x.

Cheng, F., Cheng, Z., 2015. Research progress on the use of plant allelopathy in agriculture and the physiological and ecological mechanisms of allelopathy. Front. Plant Sci. 6, 1020. https://doi.org/10.3389/fpls.2015.01020.

Chopin, T., Cooper, J.A., Reid, G., Cross, S., Moore, C., 2012. Open-water integrated multi-trophic aquaculture: environmental biomitigation and economic diversification of fed aquaculture by extractive aquaculture. Rev. Aquac. 4, 209–220. https://doi.org/10.1111/j.1753-5131.2012.01074.x.

Dai, M., Guo, X., Zhai, W., Cai, W., 2006. Oxygen depletion in the upper reach of the Pearl River estuary during a winter drought. Mar. Chem. 102, 159–169. https://doi.org/10.1016/j.marchem.2005.09.020.

Dai, M., Wang, L., Guo, X., Zhai, W., Li, Q., He, B., Gao, S., 2008. Nitrification and inorganic nitrogen distribution in a large perturbed river/estuarine system: the Pearl River Estuary, China. Biogeosciences 5, 1227–1244. https://doi.org/10.5194/bg-5-1227-2008.

Dai, M., Zhao, Y., Chai, F., Chen, M., Chen, N., Chen, Y., Cheng, D., Gan, J., Guan, D., Hong, Y., Huang, J., Lee, Y., Leung, K.M.Y., Lim, P.E., Lin, S., Lin, X., Liu, X., Liu, Z., Luo, Y.-W., Meng, F., Sangmanee, C., Shen, Y., Uthaipan, K., Wan Talaat, W.I.A., Wan, X.S., Wang, C., Wang, D., Wang, G., Wang, S., Wang, Y., Wang, Y., Wang, Z., Wang, Z., Xu, Y., Yang, J.-Y.T., Yang, Y., Yasuhara, M., Yu, D., Yu, J., Yu, L., Zhang, Z., Zhang, Z., 2023. Persistent eutrophication and hypoxia in the coastal ocean. In: Cambridge Prisms: Coastal Futures, pp. 1–71. https://doi.org/10.1017/cft.2023.7.

Diana, J.S., Egna, H.S., Chopin, T., Peterson, M.S., Cao, L., Pomeroy, R., Verdegem, M., Slack, W.T., Bondad-Reantaso, M.G., Cabello, F., 2013. Responsible aquaculture in 2050: valuing local conditions and human innovations will be key to success. BioScience 63, 255–262. https://doi.org/10.1525/bio.2013.63.4.5.

FAO, 2021. FAO Yearbook: Fishery and Aquaculture Statistics 2019. Rome. 2022.12.18 download. https://doi.org/10.4060/cb7874t.

Fong, P., Zedler, J.B., 1993. Temperature and light effects on the seasonal succession of algal communities in shallow coastal lagoons. J. Exp. Mar. Biol. Ecol. 171, 259–272. https://doi.org/10.1016/0022-0981(93)90008-c.

Froelich, P.N., 1988. Kinetic control of dissolved phosphate in natural rivers and estuaries: a primer on the phosphate buffer mechanism. Limnol. Oceanogr. 33, 649–668. https://doi.org/10.4319/lo.1988.33.4_part_2.0649.

Gordon, D.C., Boudreau, P., Mann, K., Ong, J., Silvert, W., Smith, S., Wattayakorn, G., Wulff, F., Yanagi, T., 1996. LOICZ biogeochemical modelling guidelines. In: LOICZ Core Project. Netherlands Institute for Sea Research, Yerseke.

Granada, L., Sousa, N., Lopes, S., Lemos, M.F.L., 2016. Is integrated multitrophic aquaculture the solution to the sectors' major challenges? A review. Rev. Aquac. 8, 283–300. https://doi.org/10.1111/raq.12093.

Guo, X., Wong, G.T.F., 2015. Carbonate chemistry in the northern South China Sea shelf-sea in June 2010. Deep-Sea Res. II Top. Stud. Oceanogr. 117, 119–130. https://doi.org/10.1016/j.dsr2.2015.02.024.

Han, A., Kao, S.J., Lin, W., Lin, Q., Han, L., Zou, W., Tan, E., Lai, Y., Ding, G., Lin, H., 2021. Nutrient budget and biogeochemical dynamics in Sansha Bay, China: a coastal bay affected by intensive mariculture. J. Geophys. Res. Biogeosci. 126. https://doi.org/10.1029/2020JG006220.

Hasan, B., Putra, I., Suharman, I., Iriani, D., 2016. Evaluation of salted trash fish as a protein source replacing fishmeal in the diet for river catfish (*Hemibagrus nemurus*). AACL-Int. J. Bioflux Soc. 9, 647–656.

He, B., Dai, M., Huang, W., Liu, Q., Chen, H., Xu, L., 2010. Sources and accumulation of organic carbon in the Pearl River Estuary surface sediment as indicated by elemental, stable carbon isotopic, and carbohydrate compositions. Biogeosciences 7, 3343–3362. https://doi.org/10.5194/bg-7-3343-2010.

He, Y., Xuan, J., Ding, R., Shen, H., Zhou, F., 2022. Influence of suspended aquaculture on hydrodynamics and nutrient supply in the coastal Yellow Sea. J. Geophys. Res. Biogeosci. 127. https://doi.org/10.1029/2021jg006633.

Huang, T.H., Chen, C.A., Lee, J., Wu, C.R., Wang, Y.L., Bai, Y., He, X., Wang, S.L., Kandasamy, S., Lou, J.Y., Tsuang, B.J., Chen, H.W., Tseng, R.S., Yang, Y.J., 2019. East China Sea increasingly gains limiting nutrient P from South China Sea. Sci. Rep. 9, 5648. https://doi.org/10.1038/s41598-019-42020-4.

Huang, Y., Ou, L., Yang, Y., 2017. Nutrient competition between macroalgae *Gracilaria lemaneiformis* and phytoplankton in coastal waters of Nan'ao Island, Guangdong. Oceanol. Limnol. Sin. 048, 806–813. https://doi.org/10.11693/hyhz20170200031.

Huo, Y., Wei, Z., Liu, Q., Yang, F., Long, L., Zhang, Q., Bi, H., He, Q., He, P., 2018. Distribution and controlling factors of phytoplankton assemblages associated with mariculture in an eutrophic enclosed bay in the East China Sea. Acta Oceanol. Sin. 37, 102–112. https://doi.org/10.1007/s13131-018-1238-9.

Ji, W.W., Yokoyama, H., Fu, J., Zhou, J., 2021. Effects of intensive fish farming on sediments of a temperate bay characterised by polyculture and strong currents. Aquacult. Rep. 19. https://doi.org/10.1016/j.aqrep.2020.100579.

Jiang, Z.B., Chen, Q.Z., Zeng, J.N., Liao, Y.B., Shou, L., Liu, J., 2012. Phytoplankton community distribution in relation to environmental parameters in three aquaculture systems in a Chinese subtropical eutrophic bay. Mar. Ecol. Prog. Ser. 446, 73–89. https://doi.org/10.3354/meps09499.

Kim, G., Kim, J.S., Hwang, D.W., 2011. Submarine groundwater discharge from oceanic islands standing in oligotrophic oceans: implications for global biological production and organic carbon fluxes. Limnol. Oceanogr. 56, 673–682. https://doi.org/10.4319/lo.2011.56.2.0673.

Labasque, T., Chaumery, C., Aminot, A., Kergoat, G., 2004. Spectrophotometric Winkler determination of dissolved oxygen: re-examination of critical factors and reliability. Mar. Chem. 88, 53–60. https://doi.org/10.1016/j.marchem.2004.03.004.

Li, P., Deng, Y., Shu, H., Lin, K., Chen, N., Jiang, Y., Chen, J., Yuan, D., Ma, J., 2019. High-frequency underway analysis of ammonium in coastal waters using an integrated syringe-pump-based environmental-water analyzer (iSEA). Talanta 195, 638–646. https://doi.org/10.1016/j.talanta.2018.11.108.

Lin, H., 2014. Tidal characteristics in the Sansha Bay of Fujian. J. Fujian Fish. 36, 306–314. https://doi.org/10.14012/j.cnki.fjsc.2014.04.003.

Lin, H., An, B., Chen, Z., Sun, Z., Chen, H., Zhu, J., Huang, L., 2016. Distribution of summertime and wintertime temperature and salinity in Sansha Bay. J. Xiamen Univ. 55, 349–356.

Lin, H., Chen, Z., Hu, J., Cucco, A., Zhu, J., Sun, Z., Huang, L., 2017. Numerical simulation of the hydrodynamics and water exchange in Sansha Bay. Ocean Eng. 139, 85–94. https://doi.org/10.1016/j.oceaneng.2017.04.031.

Lin, H., Chen, Z., Hu, J., Cucco, A., Sun, Z., Chen, X., Huang, L., 2019. Impact of cage aquaculture on water exchange in Sansha Bay. Cont. Shelf Res. 188, 103963. https://doi.org/10.1016/j.csr.2019.103963.

Liu, W., Han, H., Zhang, W., 2022. Current situation analysis and further improvement strategy of large yellow croaker industry in Ningde, China. Fisheries 555, 77–82.

Luo, X.S., Tang, A.H., Shi, K., Wu, L.H., Li, W.Q., Shi, W.Q., Shi, X.K., Erisman, J.W., Zhang, F.S., Liu, X.J., 2014. Chinese coastal seas are facing heavy atmospheric nitrogen deposition. Environ. Res. Lett. 9, 095007. https://doi.org/10.1088/1748-9326/9/9/095007.

Marinho-Soriano, E., Panucci, R.A., Carneiro, M., Pereira, D.C., 2009. Evaluation of *Gracilaria caudata* J. Agardh for bioremediation of nutrients from shrimp farming wastewater. Bioresour. Technol. 100, 6192–6198. https://doi.org/10.1016/j.biortech.2009.06.102.

Martinez-Porchas, M., Martinez-Cordova, L.R., 2012. World aquaculture: environmental impacts and troubleshooting alternatives. Sci. World J. 2012, 389623. https://doi.org/10.1100/2012/389623.

Martin-Jézéquel, V., Hildebrand, M., Brzezinski, M.A., 2003. Silicon metabolism in diatoms: implications for growth. J. Phycol. 36, 821–840. https://doi.org/10.1046/j.1529-8817.2000.00019.x.

Nederlof, M.A.J., Verdegem, M.C.J., Smaal, A.C., Jansen, H.M., 2021. Nutrient retention efficiencies in integrated multi-trophic aquaculture. Rev. Aquac. 14, 1194–1212. https://doi.org/10.1111/raq.12645.

Olsen, Y., Olsen, L., 2008. Environmental impact of aquaculture on coastal planktonic ecosystems, fisheries for global welfare and environment. In: Memorial Book of the 5th World Fisheries Congress.

Peng, T., Zhu, Z., Du, J., Liu, J., 2021. Effects of nutrient-rich submarine groundwater discharge on marine aquaculture: a case in Lianjiang, East China Sea. Sci. Total Environ. 786, 147388. https://doi.org/10.1016/j.scitotenv.2021.147388.

Qi, J., Yin, B., Zhang, Q., Yang, D., Xu, Z., 2016. Seasonal variation of the Taiwan Warm Current Water and its underlying mechanism. Chin. J. Oceanol. Limnol. 35, 1045–1060. https://doi.org/10.1007/s00343-017-6018-4.

Qi, Z., Shi, R., Yu, Z., Han, T., Li, C., Xu, S., Xu, S., Liang, Q., Yu, W., Lin, H., Huang, H., 2019. Nutrient release from fish cage aquaculture and mitigation strategies in Daya Bay, southern China. Mar. Pollut. Bull. 146, 399–407. https://doi.org/10.1016/j.marpolbul.2019.06.079.

Redfield, A.C., Ketchum, B.H., Richards, F.A., 1963. The Influence of Organisms on the Composition of Sea-Water, the Sea: Ideas and Observations on Progress in the Study of the Seas. Wiley Interscience, New York.

Schneider, O., Sereti, V., Eding, E.H., Verreth, J.A.J., 2005. Analysis of nutrient flows in integrated intensive aquaculture systems. Aquac. Eng. 32, 379–401. https://doi.org/10.1016/j.aquaeng.2004.09.001.

Skriptsova, A.V., Miroshnikova, N.V., 2011. Laboratory experiment to determine the potential of two macroalgae from the Russian Far-East as biofilters for integrated multi-trophic aquaculture (IMTA). Bioresour. Technol. 102, 3149–3154. https://doi.org/10.1016/j.biortech.2010.10.093.

Song, Y., Li, M., Fang, Y., Liu, X., Yao, H., Fan, C., Tan, Z., Liu, Y., Chen, J., 2023. Effect of cage culture on sedimentary heavy metal and water nutrient pollution: case study in Sansha Bay, China. Sci. Total Environ. 899, 165635. https://doi.org/10.1016/j.scitotenv.2023.165635.

Su, J., Dai, M., He, B., Wang, L., Gan, J., Guo, X., Zhao, H., Yu, F., 2017. Tracing the origin of the oxygen-consuming organic matter in the hypoxic zone in a large eutrophic estuary: the lower reach of the Pearl River Estuary, China. Biogeosciences 14, 4085–4099. https://doi.org/10.5194/bg-14-4085-2017.

Subasinghe, R., Soto, D., Jia, J., 2009. Global aquaculture and its role in sustainable development. Rev. Aquac. 1, 2–9. https://doi.org/10.1111/j.1753-5131.2008.01002.x.

Sugiura, S.H., Marchant, D.D., Kelsey, K., Wiggins, T., Ferraris, R.P., 2006. Effluent profile of commercially used low-phosphorus fish feeds. Environ. Pollut. 140, 95–101. https://doi.org/10.1016/j.envpol.2005.06.020.

Verdegem, Eding, Rooij, Verreth, 1999. Comparison of effluents from pond and recirculating production systems receiving formulated diets. World Aquacult. 30, 28–33.

Wang, C.D., Olsen, Y., 2023. Quantifying regional feed utilization, production and nutrient waste emission of Norwegian salmon cage aquaculture. Aquac. Environ. Interact. 15, 231–249. https://doi.org/10.3354/aei00463.

Wang, G., Han, A., Chen, L., Tan, E., Lin, H., 2018. Fluxes of dissolved organic carbon and nutrients via submarine groundwater discharge into subtropical Sansha Bay, China. Estuar. Coast. Shelf Sci. 207, 269–282. https://doi.org/10.1016/j.ecss.2018.04.018.

Wang, H., Dai, M., Liu, J., Kao, S.J., Zhang, C., Cai, W.J., Wang, G., Qian, W., Zhao, M., Sun, Z., 2016. Eutrophication-driven hypoxia in the East China Sea off the Changjiang Estuary. Environ. Sci. Technol. 50, 2255–2263. https://doi.org/10.1021/acs.est.5b06211.

Wang, X., Olsen, L.M., Reitan, K.I., Olsen, Y., 2012. Discharge of nutrient wastes from salmon farms: environmental effects, and potential for integrated multi-trophic aquaculture. Aquac. Environ. Interact. 2, 267–283. https://doi.org/10.3354/aei00044.

Wei, Z., You, J., Wu, H., Yang, F., Long, L., Liu, Q., Huo, Y., He, P., 2017. Bioremediation using *Gracilaria lemaneiformis* to manage the nitrogen and phosphorous balance in an integrated multi-trophic aquaculture system in Yantian Bay, China. Mar. Pollut. Bull. 121, 313–319. https://doi.org/10.1016/j.marpolbul.2017.04.034.

Wu, H., Huo, Y., Hu, M., Wei, Z., He, P., 2015. Eutrophication assessment and bioremediation strategy using seaweeds co-cultured with aquatic animals in an enclosed bay in China. Mar. Pollut. Bull. 95, 342–349. https://doi.org/10.1016/j.marpolbul.2015.03.016.

Xie, B., Huang, J., Huang, C., Wang, Y., Shi, S., Huang, L., 2020. Stable isotopic signatures ($\delta^{13}C$ and $\delta^{15}N$) of suspended particulate organic matter as indicators for fish cage culture pollution in Sansha Bay, China. Aquaculture 522, 735081. https://doi.org/10.1016/j.aquaculture.2020.735081.

Xie, B., Huang, C., Wang, Y., Zhou, X., Peng, G., Tao, Y., Huang, J., Lin, X., Huang, L., 2021. Trophic gauntlet effects on fisheries recovery: a case study in Sansha Bay, China. Ecosyst. Health Sustain. 7. https://doi.org/10.1080/20964129.2021.1965035.

Yan, S., Cao, P., 1997. Mineral characteristics of Sansha Bay and its sediment resources. J. Oceanogr. Taiwan Strait 16, 128–134.

Yang, J., Wu, D., Lin, X., 2008. On the dynamics of the South China Sea Warm Current. J. Geophys. Res. 113. https://doi.org/10.1029/2007jc004427.

Yang, Y.F., Fei, X.G., Song, J.M., Hu, H.Y., Wang, G.C., Chung, I.K., 2006. Growth of *Gracilaria lemaneiformis* under different cultivation conditions and its effects on nutrient removal in Chinese coastal waters. Aquaculture 254, 248–255. https://doi.org/10.1016/j.aquaculture.2005.08.029.

Zhai, W.-D., Chen, J.-F., Jin, H.-Y., Li, H.-L., Liu, J.-W., He, X.-Q., Bai, Y., 2014. Spring carbonate chemistry dynamics of surface waters in the northern East China Sea: water mixing, biological uptake of CO_2, and chemical buffering capacity. J. Geophys. Res. Oceans 119, 5638–5653. https://doi.org/10.1002/2014jc009856.

Zhang, G., Zhang, J., Liu, S., 2007. Characterization of nutrients in the atmospheric wet and dry deposition observed at the two monitoring sites over Yellow Sea and East China Sea. J. Atmos. Chem. 57, 41–57. https://doi.org/10.1007/s10874-007-9060-3.

Zhang, J.Z., Fischer, C.H., Ortner, P.B., 1999. Optimization of performance and minimization of silicate interference in continuous flow phosphate analysis. Talanta 49, 293–304. https://doi.org/10.1016/S0039-9140(98)00377-4.

Zhang, Y., Chai, F., Zhang, J., Ding, Y., Bao, M., Yan, Y., Li, H., Yu, W., Chang, L., 2022. Numerical investigation of the control factors driving Zhe-Min Coastal Current. Acta Oceanol. Sin. 41, 127–138. https://doi.org/10.1007/s13131-021-1849-4.

Zhao, Y., Liu, J., Uthaipan, K., Song, X., Xu, Y., He, B., Liu, H., Gan, J., Dai, M., 2020. Dynamics of inorganic carbon and pH in a large subtropical continental shelf system: interaction between eutrophication, hypoxia, and ocean acidification. Limnol. Oceanogr. https://doi.org/10.1002/lno.11393.